A STUDY OF THE BACKGROUND CORONA NEAR SOLAR MINIMUM

KUNIJI SAITO, ARTHUR I. POLAND, and RICHARD H. MUNRO

High Altitude Observatory, National Center for Atmospheric Research, Boulder, Colo., U.S.A.*

(Received 21 April, 1977)

Abstract. The white light coronagraph data from Skylab is used to investigate the equatorial and polar K and F coronal components during the declining phase of the solar cycle near solar minimum. Measurements of coronal brightness and polarization brightness product between 2.5 and $5.5R_\odot$ during the period of observation (May 1973 to February 1974) lead to the conclusions that: (1) the equatorial corona is dominated by either streamers or coronal holes seen in projections on the limb approximately 50% and 30% of the time, respectively; (2) despite the domination by streamers and holes, two periods of time were found which were free from the influences of streamers or holes (neither streamers nor holes were within 30° in longitude of the limb); (3) the derived equatorial background density model is less than 15% below the minimum equatorial models of Newkirk (1967) and Saito (1970); (4) a spherically symmetric density model for equatorial coronal holes yields densities one half those of the background density model; and (5) the inferred brightness of the F-corona is constant to within ±10% and ±5% for the equatorial and polar values, respectively, over the observation period. While the F-corona is symmetric at $2R_\odot$ it begins to show increasing asymmetry beyond this radius such that at $5R_\odot$ the equatorial F-coronal brightness is 25% greater than the polar brightness.

1. Introduction

One of the fundamental goals of solar physics is to understand the physical processes which govern mass and energy flow in the solar corona. Before such processes can be studied, the physical properties which characterize the corona (e.g., the density, temperature, magnetic field) must be ascertained. One area of particular importance is the frequently used concept of a background corona: a component of the corona distinct from either streamers or coronal holes. Not only have background coronal models been used to estimate the densities of coronal features from white light eclipse observations over the past 75 years (see for example, Baumbach, 1937; van de Hulst, 1950; Newkirk, 1967; and Saito, 1970), the models have also played a fundamental role in the interpretation of solar radio emission and in the study of outward flowing coronal material into the solar wind. Models calculated in past work have indicated that the corona varies, depending upon the phase of the solar cycle; it is axisymmetric about the poles near solar minimum, and spherically symmetric and more dense near solar maximum.

The major uncertainty in previous calculations of the background coronal density results from the use of eclipse measurements. Since each eclipse can provide at most only a few hours of observation of the solar corona, it is not possible to assess the contribution to measured coronal radiation from streamers far from the solar limb but still along the line of sight. This possible presence of streamers raises the question

* The National Center for Atmospheric Research is sponsored by the National Science Foundation.

Solar Physics **55** (1977) 121–134.

as to whether or not any given measurements accurately represent only the background corona. To reduce the influence of this effect, Saito (1970) averaged measurements of regions in the corona, apparently not containing streamers, from several eclipses to produce his background density model. The weakness of this approach lies in the difficulty in achieving an accurate cross calibration between the various data sets, obtained under widely varying conditions.

This paper presents a reinvestigation of the concept of a background coronal density for a period approximately two years prior to solar minimum (May 1973 to February 1974) using the High Altitude Observatory's (HAO) white light coronagraph data from Skylab (see MacQueen *et al.*, 1974). The essentially continuous photographic measurement of the outer corona afforded by the Skylab coronagraph permits the selection of regions in the corona free from streamers and coronal holes. Specifically, for the determination of the background corona only data are used when no streamer and no coronal hole is within ±30° of the limb, e.g., within ±2.5 days of limb passage.

The use of the Skylab data also permits a more accurate separation of the *F*-corona beyond $3R_\odot$. Since the data were obtained above the Earth's atmosphere, they are free from the variability and polarization of the sky background which affect eclipse observations. The lack of sky interference and reduced stray light levels beyond $3R_\odot$ in this data permit more sensitive polarimetry at low light levels and thus a more accurate separation of the *K*-corona from the dominant *F*-corona in lower density coronal regions.

In Section 2 of this paper the observational data are presented in a form suitable for the calculation of *K* and *F* coronal models, while in Section 3 the method used for calculating density models is discussed and the results from these calculations for the equatorial background, equatorial holes, and polar holes are presented. Finally, in the last section the results are discussed with respect to the reliability of the derived background model and the fractions of time streamers (50%), holes (30%), and background (20%) brightness are observed on the limb.

2. Observational Data

In this section we present the HAO coronagraphic data in a form suitable for the study of the *K* and *F* coronal components at the equator and poles. The instrument, described in detail by MacQueen *et al.* (1974), was capable of obtaining broad-band (3500–7000 Å) coronal images through one unpolarized and three linear polaroid filters. Except for three gaps of several days (10–18 June, 16–28 July, and 15–17 November) due to instrument and Skylab malfunctions, the data permit the determination of the brightness and polarization in the solar corona between 2 and $6R_\odot$ at a rate of at least once a day from 28 May 1973 to 3 February 1974. To separate the polarized *K* and unpolarized *F* coronal components (see van de Hulst, 1950; Blackwell *et al.*, 1967), it is necessary to analyze the brightness (B) and the polarization times brightness (pB) as functions of position (apparent height ρ and

position angle) and time. Measurements of pB are used to calculate a K-coronal model which in turn is subtracted from the total measured brightness B to obtain the F-coronal brightness.

A sample unpolarized image used in this analysis is shown in Figure 1. The photographic image consists of vignetted K and F coronal radiances plus intrumentally produced stray light. The stray light (which, for example, has a range of 2 to $3\times10^{-10}\,\bar{B}_\odot$ at $3R_\odot$, where $\bar{B}_\odot$ is the mean brightness of the solar disk) has been determined as a function of position within the instrument's field of view (Csoeke-Poeckh *et al.*, 1977). After the stray light is removed from the total signal, the correction for instrumental vignetting is applied (for instance, the instrumental transmission is 39% at $3R_\odot$). The resulting coronal brightness, $B = B_K + B_F$, is then tabulated for selected heights between 2.5 and $5.5R_\odot$. A plot of the corrected coronal brightness for Figure 1 is presented in Figure 2 at 2.5, 2.7, 3.0, 4.0 and $5.5R_\odot$. The data gap over the south polar region (PA = 180°) is a result of shadowing by the support for the instrument's occulting disks. For times during the Skylab period when astronauts rotated the instrument 90°, additional images of the south polar region were acquired.

The polarization brightness (pB), as well as an independent measure of the total coronal brightness (B), are calculated from a combination of images obtained through three polaroid filters at different orientations. Since pB is a measure of only linearly polarized light and the stray light is essentially unpolarized, pB signals are

Fig. 1. Sample coronal image for day of year 152 (1 June 1973). North is at the top (PA = 0°) and east to the left (PA = 90°).

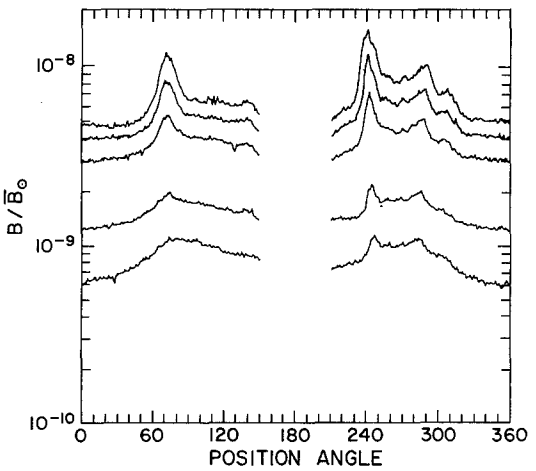

Fig. 2. Coronal brightness (B_{K+F}) as a function of position angle at heights of 2.5, 2.7, 3.0, 4.0, and 5.5$R_\odot$ for the coronal image presented in Figure 1. The missing data between 150° and 210° results from a support for the occulting disks.

only corrected for instrument vignetting. A plot of the corrected pB signals for Figure 1 is presented in Figure 3. Since pB is obtained by appropriate differencing of polarized images, it is intrinsically noisier than B; thus to improve the signal-to-noise the pB data represents a 2′ area instead of the 24″ area used for the B data.

To investigate the influence of streamers and holes in the measurement of the background corona, the coronal brightness distribution was obtained once per day during the Skylab period while the pB information was determined for approximately every other day. From this data set, B and pB values as a function of height

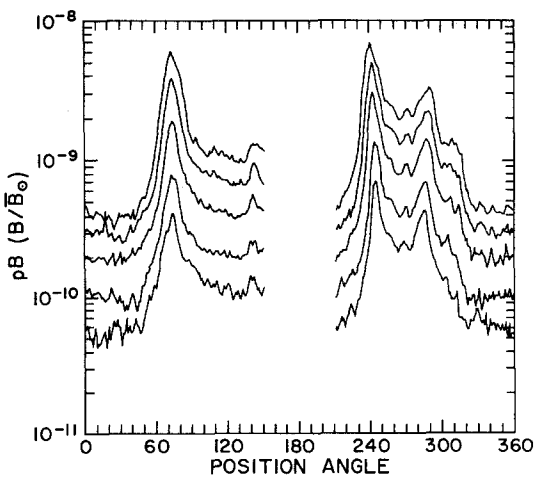

Fig. 3. Polarization brightness (pB) as a function of position angle for the same heights and time as in Figure 2.

were compiled at selected position angles including the eastern equator (PA = 90°) and western equator (PA = 270°) for the entire observational period. A sample of these data is illustrated in Figure 4 for the western equator at $3R_\odot$. For the brightness measurements, determinations from both clear (crosses) and polarized (circles) images are presented; coincident values are represented by circles only.

In Figure 4, significant fluctuations, factors of 2 and 5, are evident in the temporal behavior of the equatorial values of B and pB respectively, but there is no systematic trend observed through the entire observational period. The evaluation of the equatorial coronal radiance over the mission period is discussed more completely in a study by MacQueen and Poland (1977). Many of the fluctuations recur at the solar synodic rate of 27 days – the highest values corresponding to observed coronal streamers and the lowest values corresponding, without exception, to the limb passages of X-ray and EUV coronal holes (Nolte *et al.*, 1976; Bohlin and Rubenstein, 1975). The west limb passages of these coronal holes are indicated by arrows in Figure 4. It is interesting to note that the magnitudes and radial gradients of the lowest pB values are nearly identical (e.g., pB at $3R_\odot$ is $4.5 \pm 1.0 \times 10^{-10} \bar{B}_\odot$ when coronal holes are on the limb).

It can be seen from Figure 5, that B and pB over the poles vary significantly less than at the equator (Figure 4). Variations in polar brightness are generally on the order of the relative photometric accuracy, ±8% (Poland *et al.*, 1977), except when

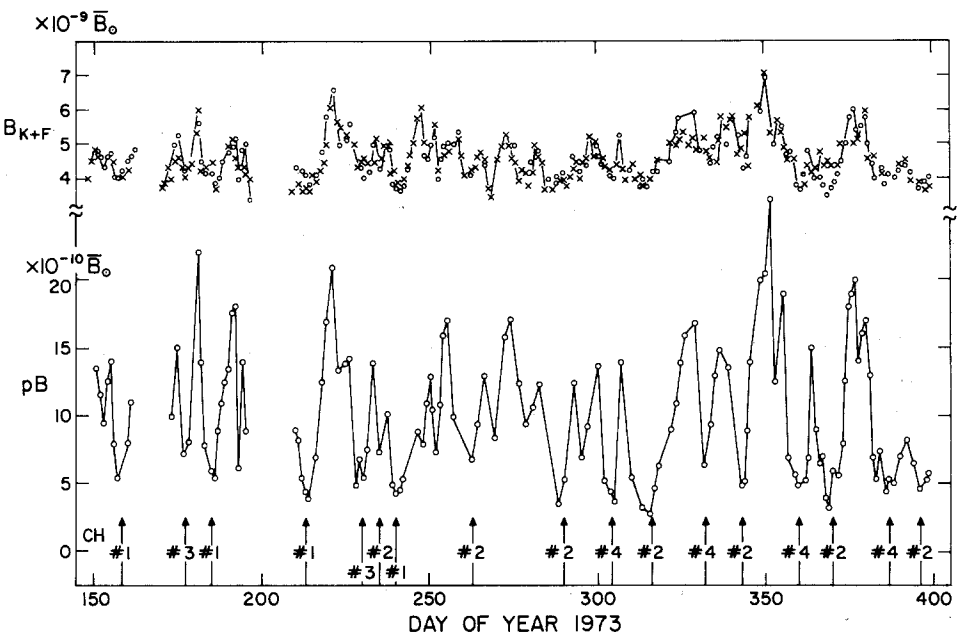

Fig. 4. Brightness (B) and polarization brightness (pB) as a function of time along the western equator (PA = 270°) at $3R_\odot$. Times of limb passages of coronal holes numbered by Nolte *et al.* (1976) are indicated by arrows.

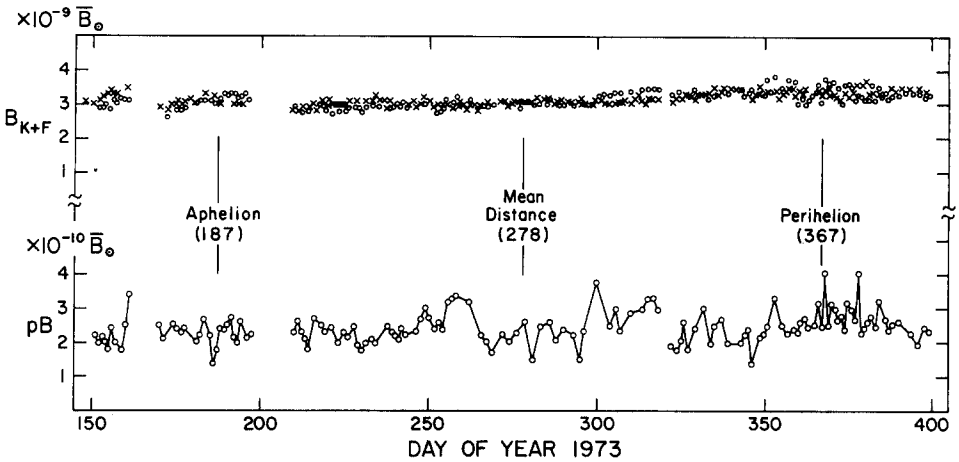

Fig. 5. Brightness (B) and polarization brightness (pB) as a function of time at $3R_\odot$ over the north pole. Times of aphelion and perihelion are noted.

high latitude streamers are observed in projection over the pole. The slight increase in the polar brightness, seen in Figure 5, of about 6% between aphelion and perihelion results from the uncorrected seasonal change in the Sun's image size, which also produces an increase in instrumentally induced stray light. The larger fluctuations in pB are due primarily to two causes: (1) noise in the derived polarization signal; and (2) high latitude streamers seen in projection over the pole.

It is difficult to accurately assess the errors present in the measurements of B and pB. The photometric calibration of the coronagraph has been discussed by Poland *et al.* (1977) who place the relative error at ±8% and the absolute accuracy at 20%. Further uncertainties are introduced through errors in the corrections for stray light (Csoeke-Poeckh *et al.*, 1977) and their amplification by the vignetting correction. The comparison of the coronal brightness calculated through unpolarized and linear polarized images reveals random deviations usually less than 20%; the source of this error is unknown. In all, we estimate that the relative and absolute brightness errors are approximately 20% and 50%, respectively, for measurements near $2.5R_\odot$; they improve by a factor of 2 near $5R_\odot$. Relative errors for pB are slightly higher since it is calculated using a differencing technique.

3. Coronal Models

The observed values of $pB(\rho)$ combined with the assumption of spherical symmetry permit the calculation of a background coronal electron density model. The integral equation for pB,

$$pB(\rho) = \tfrac{3}{4}\bar{B}_\odot \sigma \int_\rho^\infty N_e(r)\{A(r) - B(r)\} \frac{\rho^2\, dr}{r(r^2-\rho^2)^{1/2}}, \qquad (1)$$

is inverted using the techniques of van de Hulst (1950) to obtain the electron density as a function of solar radius, $N_e(r)$, from the observed pB values. In Equation (1) ρ is the apparent height above the solar limb and r is the distance from Sun center. The K-coronal brightness calculated from this density model is then subtracted from the measured brightness to produce an F-coronal brightness model.

Coronal density models are presented for three cases where spherical symmetry is justified: (1) the case where equatorial data are unaffected by either streamers or holes; (2) the case where equatorial coronal holes were on the limb; and (3) polar regions. The model for coronal holes is primarily intended to show their possible influence on background model calculations, although it is probably a good approximation to the radial density distribution in equatorial holes. The polar hole model is used for comparison with the work of Munro and Jackson (1977) and for the calculation of the polar F-coronal brightness.

3.1. Technique for constructing density models

The specification of the electron density as a function of radius is accomplished in several steps. Following van de Hulst (1950), the observed values of pB are expressed in the functional form

$$pB(\rho)_{\text{obs}} = a_1\rho^{-b_1} + a_2\rho^{-b_2}, \tag{2}$$

where the coefficients a_i and b_i are selected through a minimization technique to reproduce the measured quantity to within ±5%. Then the integral Equation (1) for pB is inverted to obtain the electron density as a function of radius,

$$N_e(r) = (a_1' r^{-b_1} + a_2' r^{-b_2}) g(r), \tag{3}$$

where $g(r)$ is a complicated expression involving the geometry of the scattering process and a_1' and a_2' are determined from the a_i's and b_i's calculated for Equation (2) (see van de Hulst, 1950). Equation (3) is then simplified by expressing the density in its final form as

$$N_e(r) = c_1 r^{-d_1} + c_2 r^{-d_2}, \tag{4}$$

where r is given in units of solar radii and c_i and d_i are calculated using a minimization technique. This procedure creates density models which, when substituted into the integral equation for pB, reproduce the measured values within ±5%.

3.2. Electron density models

Examination of the pB data and unpolarized photographs of the corona indicated that there were only two periods of 5 days each during the Skylab mission when the equatorial limbs were free from streamers and coronal holes. These periods were centered around DOY 266 and DOY 283 and both occurred on the east limb; note that this is significantly less than one Carrington rotation and thus involved two separate areas on the Sun. We feel that these data yield the most reliable determination of the background corona. The electron density model, labeled 'Background' in

Figure 6 was obtained from the analysis of these two periods and is less than 15% below the Newkirk (1967) and Saito (1970) models (these latter two similar models are henceforth referred to as the Newkirk-Saito model). This difference is not considered to be significant since it may result from either absolute calibration differences or the influence of streamers in the earlier work.

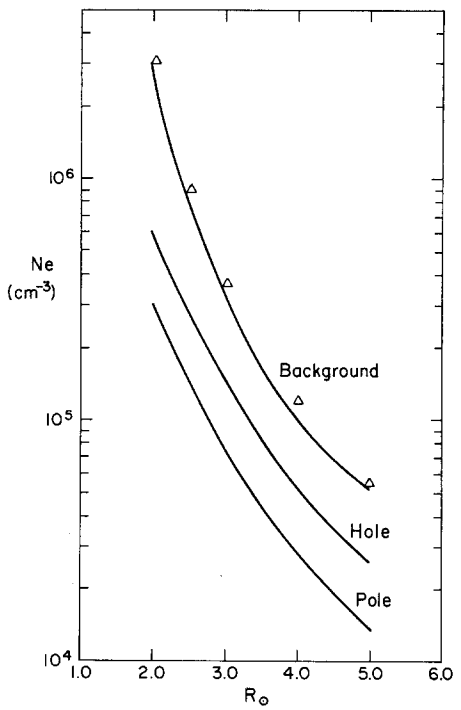

Fig. 6. Electron density models as a function of radius for the equatorial background, equatorial coronal holes, and the polar holes. The Newkirk-Saito minimum equatorial background is indicated by triangles.

To determine the effect coronal holes have on what could be inferred as the background coronal density, a model was calculated using *pB* values measured for times when coronal holes were on the equatorial limb. The times were selected using the location of X-ray and EUV coronal holes (see Figure 4). Under the assumption of spherical symmetry, the density model derived from this procedure (designated as 'Hole' in Figure 6) is approximately a factor of two lower than the background model density. Since the *pB* data for all the holes has a scatter of less than 25%, the conditions existing in various equatorial coronal holes are probably very similar. Although the assumption of spherical symmetry used in this calculation may lead to errors in the inferred density, the large volumes occupied by coronal holes above $2R_\odot$ (Munro and Jackson, 1977) minimize the effect of other coronal features surrounding a specific coronal hole. Hence it is believed that this electron density distribution is representative of equatorial coronal holes.

A spherically symmetric density model for the solar poles was also obtained for comparison with previous studies and to permit the calculation of the polar *F*-coronal brightness. The model, labeled 'Pole' in Figure 6, is about a factor of 4 below the equatorial background densities and is approximately 15% more dense than a similar polar coronal hole model of Munro and Jackson (1977). The 15% difference is ascribed to Munro and Jackson's use of data free from the projection of high latitude streamers over the pole. However, it can be seen from Figure 5 that the variation in the polar data throughout the period of observation was small and indicates that the corona over the solar poles can be adequately represented by a temporally invariant density model.

The electron density models discussed above are summarized in Table I. The coefficients for expressing pB as a function of apparent height ρ (Equation (2)) and the derived spherically symmetric density distribution (Equation (4)) are supplied as an aid to obtaining values at any radius. Note that the coronal density expressions have been derived for data between 2.5 and $5.5R_\odot$ and do not necessarily represent true coronal densities outside these limits.

The numerical results for the background equatorial model are presented in Table II. In columns 2 through 4 the calculated values of N_e, pB and B_K are presented as a function of radius. The numbers in parentheses are extrapolated quantities and are only presented for comparison. The values for the electron density from the Newkirk-Saito model are presented in column 7. It is seen that the new electron density model, even when extrapolated, is less than 15% below the Newkirk-Saito model. Table III gives numerical values for both spherically symmetric and axisymmetric polar models. For the axisymmetric model, the latitudinal variation of the electron density given by Munro and Jackson (1977) was used to match the observed pB variation in the polar region. This latitudinal distribution requires the density directly over the pole to be about 25% less than that derived for the spherically symmetric model. While both models produce identical pB values directly over the pole, the *K*-coronal brightness of the axisymmetric model is 10% higher.

3.3. *F*-CORONAL MODELS

It is possible to determine the *F*-coronal brightness by subtracting the *K*-coronal brightness (calculated from model electron density distributions) from the observed coronal brightness, *B*. Equatorial *F*-coronal models are calculated for data obtained when streamers did not dominate the limb (i.e., B_K did not exceed the background B_K by more than 20%). The variation in the total brightness plotted in Figure 4 is essentially identical to the calculated *K*-coronal brightness variation. Thus we conclude that the equatorial *F*-coronal brightness is the same on both limbs and is constant to within ±10% over the Skylab period. The derived average equatorial *F*-coronal brightness is presented in Figure 7 and Table II.

The *F*-coronal dominance is most evident over the pole where the *F*-corona is more intense than the *K*-corona by more than an order of magnitude. Thus polar brightness essentially reflects the behavior of the *F*-corona itself. As discussed in

TABLE I

Coefficients for binomial expressions for pB and the derived spherically symmetric density distribution. See Equations (2) and (4)

	pB			
Model	a_1	b_1	a_2	b_2
Background (equator)	1.20×10^{-8}	3.07	9.86×10^{-7}	6.95
Equatorial hole	2.33×10^{-9}	4.29	4.43×10^{-8}	4.29
Polar regions (hole)	4.36×10^{-9}	3.60	2.32×10^{-8}	4.67
	N_e			
Model	c_1	d_1	c_2	d_2
Background (equator)	$1.36\times10^{+6}$	2.14	$1.68\times10^{+8}$	6.13
Equatorial hole	$5.27\times10^{+6}$	3.30	$3.54\times10^{+6}$	5.80
Polar regions (hole)	$3.15\times10^{+6}$	4.71	$1.60\times10^{+6}$	3.01

TABLE II

Equatorial coronal background model

r	N_e	pB	B_K	B_{K+F}	B_F	N_e *Newkirk-Saito*
1.5	(1.46×10^{7})	(5.8×10^{-8})	(1.1×10^{-7})			1.53×10^{7}
2.0	(2.71×10^{6})	(9.3×10^{-9})	(1.5×10^{-8})			2.92×10^{6}
2.5	8.02×10^{5}	2.4×10^{-9}	3.7×10^{-9}	8.9×10^{-9}	5.2×10^{-9}	9.02×10^{5}
3.0	3.29×10^{5}	8.9×10^{-10}	1.4×10^{-9}	4.7×10^{-9}	3.3×10^{-9}	3.78×10^{5}
4.0	1.04×10^{5}	2.3×10^{-10}	3.7×10^{-10}	1.9×10^{-9}	1.5×10^{-9}	1.17×10^{5}
5.0	5.21×10^{4}	9.9×10^{-11}	1.6×10^{-10}	1.1×10^{-9}	9.2×10^{-10}	5.50×10^{4}
6.0	(3.22×10^{4})	(5.2×10^{-11})	(8.5×10^{-11})			3.19×10^{4}

Section 2, the temporal behavior of the polar brightness (see Figure 5) implies that the F-corona remains constant to within ±5% over the 8 month Skylab period. The polar F-coronal model was calculated in the same manner as the equatorial model and the results are presented in Figure 7 and Table III. The polar F-coronal model agrees with that given by Allen (1963) to within 5%.

Although the equatorial and polar F-coronal models are nearly identical at small heights, the brightness distribution becomes increasingly oblate beyond $2R_\odot$. In Figure 8 the ellipticity, defined as

$$\varepsilon = \frac{r_{\text{equ}} - r_{\text{pol}}}{r_{\text{equ}}}, \tag{5}$$

where r_{equ} and r_{pol} are the radius vectors along the equator and pole corresponding to identical F-coronal brightnesses, is shown as a function of r_{equ}. This is to be contrasted with Allen's model which assumes the F-corona to be spherically symmetric. The ellipticity shown in Figure 8 is observed to continue its increase into the zodical light (Blackwell *et al.*, 1967).

TABLE III

Spherically symmetric polar model

r	N_e	pB	B_K	B_{K+F}	B_F
2.0	(3.19×10^{5})	(1.3×10^{-9})	(2.2×10^{-9})		
2.5	1.44×10^{5}	4.8×10^{-10}	7.8×10^{-10}	5.5×10^{-9}	4.7×10^{-9}
3.0	7.64×10^{4}	2.2×10^{-10}	3.5×10^{-10}	3.0×10^{-9}	2.6×10^{-9}
4.0	2.93×10^{4}	6.5×10^{-11}	9.9×10^{-11}	1.4×10^{-9}	1.3×10^{-9}
5.0	(1.42×10^{4})	(2.6×10^{-11})	(3.9×10^{-11})	7.4×10^{-10}	7.0×10^{-10}

Axisymmetric polar values

r	N_e	pB	B_K	B_{K+F}	B_F
2.0	(2.47×10^{5})	(1.3×10^{-9})	(2.4×10^{-9})		
2.5	1.11×10^{5}	4.8×10^{-10}	8.8×10^{-10}	5.5×10^{-9}	4.6×10^{-9}
3.0	5.91×10^{4}	2.2×10^{-10}	3.9×10^{-10}	3.0×10^{-9}	2.6×10^{-9}
4.0	2.27×10^{4}	6.5×10^{-11}	1.1×10^{-10}	1.4×10^{-9}	1.3×10^{-9}
5.0	(1.10×10^{4})	(2.6×10^{-11})	(4.5×10^{-11})	7.4×10^{-10}	7.0×10^{-10}

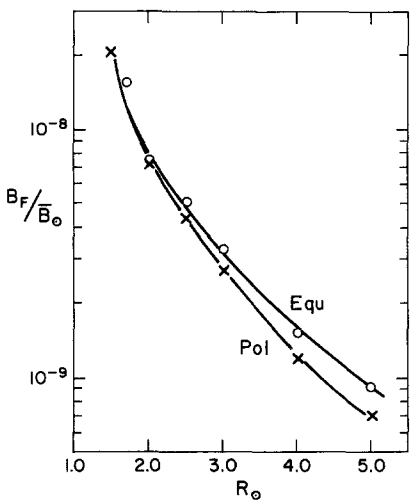

Fig. 7. Derived F-coronal brightness over the equator and the poles.

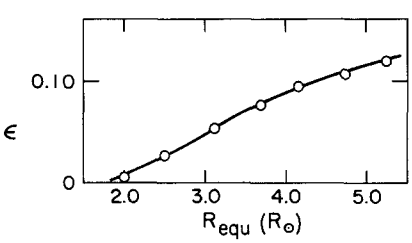

Fig. 8. Ellipticity of the F-corona as given in Equation (5).

4. Discussion

That streamers, coronal holes, and the background corona produce great variations in measured pB values at the equator can be seen from Figure 4. With the background corona defined, it is possible to divide the measured pB values into three groups: (1) All pB values greater than 20% above the background – these are assumed to be influenced or dominated by streamers; (2) All pB values more than 20% below the background – these are assumed to be influenced or dominated by coronal holes; and (3) Values within 20% of the background – these can either truly represent the background corona or can be due to fortuitous combinations of coronal holes and streamers. The average pB values for each of the above groups of data are presented in Figure 9. It is of interest to note that the radial gradients for each group are almost identical.

The fraction of time that each group was measured on the limb is approximately: 50% streamer-influenced; 30% hole-influenced; and 20% background-like radiance. While these measures do not give the volume fraction of the corona filled with streamers, holes, and background, they do indicate how little of the corona above $2R_\odot$ can be considered as 'background'. Since 60% of the solar sphere above $2R_\odot$ is dominated by polar holes at this time (Munro and Jackson, 1977), and if we

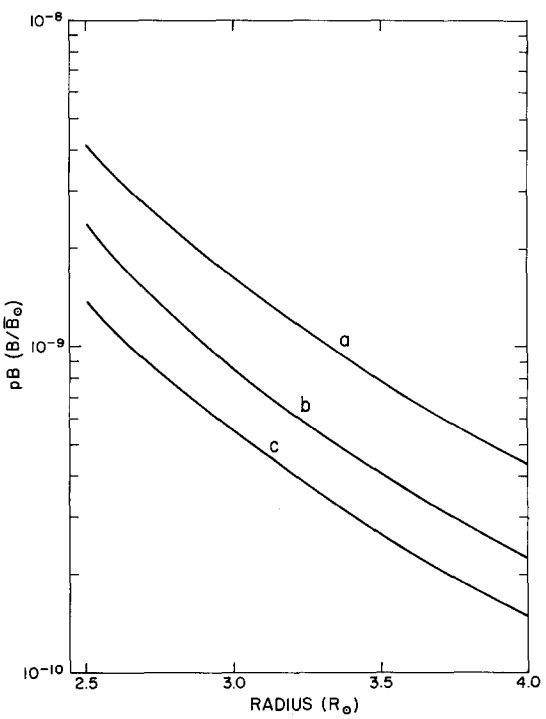

Fig. 9. Polarization brightness (pB) as a function of height for (a) the mean of all the data greater than 20% above background; (b) the mean of all the data within 20% of the background and; (c) the mean of all the data more than 20% below the background.

interpret the remaining equatorial volume (40%) as consisting of at least 30% holes, then we estimate that at least 70% of the coronal volume above $2R_\odot$ is filled with coronal holes. A more specific determination of the volume fractions would require the three dimensional specification of the entire coronal density distribution. However, the small fraction of the corona that can be considered to be background during this period of the solar cycle is further emphasized by the fact that out of 227 days of observation, only two relatively short periods could be found that were definitely free from the effects of streamers and holes.

In view of the large variation in coronal density at a given height between holes and background, one might question the significance of using a single density distribution to describe the solar corona. At any given height the density difference between a hole and the background is at least a factor of 2; between background and streamers it is even greater. If density is used to define a height in the corona (as with radio burst analysis), a given density can be found at heights that differ by $1R_\odot$ between holes and the background; this difference is even greater for streamers. Thus, the use of a single density model is potentially misleading.

In contrast to the variability of the *K*-corona, the *F*-corona is very constant. The variations in B due to *K*-coronal features are consistently compensated for in the calculated electron coronal brightness such that the derived equatorial *F*-coronal brightness (i.e., $B_F = B - B_K$) is constant. The polar *F*-corona is also constant with time but has a slightly steeper radial gradient than the equatorial *F*-corona. While the *F*-corona is symmetric about the Sun at $2R_\odot$, it becomes increasingly more asymmetric with radius – attaining an ellipticity of 12% at $5R_\odot$.

In summary, the concept of a background corona seems to be a valid one although other coronal features make its properties difficult to measure. The radial density distribution for the coronal background derived from the HAO coronagraph data is essentially the same as, but systematically lower than, that found in previous studies. However, at this particular phase of the solar cycle (declining, but near solar minimum), a substantial fraction of the equatorial corona consists of coronal holes above $2R_\odot$ and we estimate that this fraction may exceed 70% of the entire solar corona when the polar coronal holes are included. The density in equatorial coronal holes is, on average, a factor of two less than the background density. Finally, although no change in the brightness of the *F*-corona can be detected during the 8 months of observations, the *F*-corona can not be considered symmetric about the Sun above about $2.5R_\odot$.

Acknowledgements

The authors recognize the many helpful discussions with Dr R. MacQueen and the help of Mr T. Blaschko, Mr A. Csoeke-Poeckh, and Mr A. Stanger in reducing the data.

This research was supported by NASA Contract NAS5-3950 to the University Corporation for Atmospheric Research.

References

Allen, C. W.: 1963, *Astrophysical Quantities*, Athlone Press, London.
Baumbach, S.: 1937, *Astron. Nachr.* **263**, 121.
Blackwell, D. E., Dewhirst, D. W., and Ingham, M. F.: 1967, *Adv. Astron. Astrophys.* **5**, 1.
Bohlin, J. D. and Rubenstein, D. M.: 1975, NOAA World Center A for Solar-Terrestrial Physics, Report UAG 51.
Csoeke-Poeckh, A., MacQueen, R. M., and Poland, A. I.: 1977, *Appl. Optics* **16**, 931.
MacQueen, R. M. and Poland, A. I.: 1977, *Solar Phys.*, in press.
MacQueen, R. M., Gosling, J. T., Hildner, E., Munro, R. H., Poland, A. I., and Ross, C. L.: 1974, *Soc. Photo-Opt. Inst. Eng.* **44**, 207.
Munro, R. H. and Jackson, B. V.: 1977, *Astrophys. J.* **213**, 874.
Newkirk, G. A., Jr.: 1967, *Ann. Rev. Astron. Astrophys.* **5**, 213.
Nolte, J. T., Krieger, A. S., Timothy, A. F., Viana, G. S., and Zombeck, M. V.: 1976, *Solar Phys.* **46**, 291.
Poland, A. I., Gosling, J. T., MacQueen, R. M., and Munro, R. H.: 1977, *Appl. Optics* **16**, 926.
Saito, K.: 1970, *Ann. Tokyo Astron. Obs., Ser. 2*, **12**, 53.
van de Hulst, H. C.: 1950, *Bull. Astron. Inst. Neth.* **11**, 135.